Use of Measured Aerosol Optical Depth and Precipitable Water to Model Clear Sky Irradiance

Mark M. Mikofski[1], Clifford W. Hansen[2], William F. Holmgren[3] and Gregory M. Kimball[1]

[1]SunPower Corporation, Richmond, CA, 94804, USA
[2]Sandia National Laboratories, Albuquerque, NM, 87185, USA
[3]University of Arizona, Tucson, AZ, 85721, USA

***Abstract* — Predicted clear sky irradiance depends on atmospheric composition as well as solar position and extra-terrestrial irradiance. The effects on clear sky irradiance of year to year variations in atmospheric composition were studied using measurements of aerosol optical depth (AOD) and precipitable water (P_{wat}) at seven locations in the United States. Three clear sky models were evaluated, including one that uses Linke turbidity (T_L). This model was evaluated using historical, static T_L as well as updated values derived from real-time AOD and P_{wat} measurements. The average annual error in predicted clear sky irradiance using static T_L did not differ significantly from year to year. Annual average error in predicted GHI was less than 5% for all models with no significant difference between models. The model with static T_L had the lowest DNI errors, and the Bird model had the smallest GHI error but the largest DNI error. On average DNI and GHI were under-predicted.**

***Index Terms* — clear sky, irradiance, aerosol optical depth, precipitable water.**

I. Introduction

Predicting clear sky irradiance is important for estimating energy generation by solar power systems. Clear sky models predict the direct normal (DNI), diffuse horizontal (DHI) and global horizontal (GHI) components of irradiance on a cloudless day. Since the concentration of aerosol and water vapor in the atmosphere can affect all three of these irradiance components, they can also influence power production. We analyzed the effects of aerosol optical depth (AOD) and precipitable water (P_{wat}) on irradiance predictions from three clear sky models by comparing them with irradiance measurements at seven US locations. This paper is a report on our analysis.

II. Methods

This section describes the differences between the clear sky models and the sources of atmospheric composition and irradiance measurements used in our analysis.

A. Clear Sky Models

Several numerical models are available for prediction of clear sky irradiance. Ineichen recently published a study of seven clear sky models [1], evaluating them using atmospheric data from the Monitoring Atmospheric Composition and Climate (MACC) project of the Copernicus Atmospheric Monitoring Service (CAMS). This data is provided by the European Center for Medium-Range Weather Forecasts (ECMWF). Ineichen concluded that the Simplified Solis model [2] demonstrated the smallest long term variance from measurements at twenty two irradiance stations mostly in Europe over an 8 year period. The National Renewable Energy Laboratory (NREL) performed a similar study [3] with irradiance and atmospheric data from the National Oceanic and Atmospheric Administration (NOAA) Earth System Research Laboratory (ESRL) Surface Radiation Network (SURFRAD) and found the Bird model [4]–[7] to be a better fit. We analyzed these models as well as the Ineichen-Perez model, popular due to its long-established implementation in PVsyst and in the PVLIB MATLAB and Python modeling libraries [8]–[10].

We compared the accuracies of Bird, Simplified Solis, and Ineichen-Perez models using PVLIB-Python. The Bird and Simplified Solis models take inputs of P_{wat} and broadband AOD measurements directly, but the Ineichen-Perez model [11], [12] uses Linke turbidity (T_L) [13] as a parameter to represent both components of the atmosphere. PVLIB-Python provides a gridded static set of monthly T_L values from 2003, obtained from the SoDa Pro website. We re-calculated the T_L values from AOD and P_{wat} measurements using the method described in the next section and compared irradiance predictions from both the static and re-calculated T_L values to demonstrate year to year variability.

B. Measurements of Atmospheric Composition

We used measurements of AOD and P_{wat} from the CAMS MACC project provided by ECMWF. This data is derived from an atmospheric model that assimilates satellite data from MODIS and is calibrated with independent ground measurements from AERONET [14]. Aerosol data at several wavelengths and total column water vapor are available over the entire globe at 0.75° increments every 3 hours from 2003 to 2012.

In our analysis, we calculated T_L from broadband AOD and P_{wat} using Eq. (1) in which AM is airmass, calculated using the NREL solar position algorithm (SPA) form PVLIB, and δ_{total}.is the total atmospheric attenuation, derived in Eq. (2).

$$T_L = -\frac{-(9.4 + 0.9AM)\log(\exp(-AM\delta_{total}))}{AM} \quad (1)$$

The method developed by Kasten [17], [18] is explained in detail by Ineichen and Perez [12], [19]. The contributions from pure Rayleigh scattering, $\delta_{Rayleigh}$, through a hypothetical "clean dry atmosphere" are combined with water absorption, δ_{water}, and the broadband AOD to get the total atmospheric attenuation, δ_{total}, in Eq. (2).

$$\delta_{total} = \delta_{Rayleigh} + \delta_{water} + \tau_{aerosol} \quad (2)$$

There are several options for determining the broadband AOD, $\tau_{aerosol}$. Molineaux [20] proposed using a single AOD measurement at 700 nm which is used in the Simplified Solis model. For the Bird model, Bird and Hulstrom [21] suggested two AOD measurements at 380 nm and 500 nm correlated by the expression in Eq. (3) where τ is AOD and λ is wavelength.

$$\tau_{aerosol} = 0.27583\tau_{\lambda=380nm} + 0.35\tau_{\lambda=500nm} \quad (3)$$

To calculate AOD at 380 nm, 500 nm and 700 nm, we obtained AOD at 550 nm and 1240 nm from the ECMWF MACC data. Then, assuming AOD is related to wavelength by the Angstrom turbidity model [15], [16], we calculated the Angstrom exponent, α, from AOD at the two wavelengths, and used α to obtain AOD at the desired wavelengths. This is demonstrated in Eq. (4).

$$\tau = \tau_0 \left(\frac{\lambda}{\lambda_0}\right)^{-\alpha} \quad (4)$$

C. Measurements of Clear Sky Irradiance

To evaluate the clear sky irradiance models and the measurement sources of AOD and P_{wat}, predictions of DNI, DHI and GHI were compared to SURFRAD measurements of irradiance, ambient temperature, relative humidity and pressure at either 1-minute or 3-minute intervals. The SURFRAD stations listed in Table I were used for the years from 2003 to 2012. Down-sampled measurements at 3-minute intervals were filtered for clear sky conditions using PVLIB-Python with a 30-minute window and clear sky calculated using Simplified Solis. Measurements below a GHI threshold of 200 W/m^2 were also removed.

Mean bias error (MBE) was calculated between the filtered measured data and the predictions using the formula in Eq. (5) in which N is the number of measurements. Relative error was obtained by dividing the calculated MBE by the average of the measurements. The analysis was done in a Python notebook that can be accessed from an online repository at https://github.com/mikofski/pvsc44-clearsky-aod.

$$MBE = \frac{\sum_{n=1}^{N}(predicted_n - measured_n)}{N} \quad (5)$$

TABLE I
SURFRAD SURFACE RADIATION STATIONS

Station Name	Station ID	Latitude	Longitude	Elevation (m)
Bondville, IL	bon	40.05	-88.37	213
Table Mountain, CO	tbl	40.13	-105.24	1689
Desert Rock, NV	dra	36.62	-116.02	1007
Fort Peck, MT	fpk	48.31	-105.10	634
Goodwin Creek, MS	gwn	34.25	-89.87	98
Penn State, PA	psu	40.72	-77.93	376
Sioux Falls, SD	sxf	43.73	-96.62	473

III. RESULTS

Fig. 1 to 4 compare monthly static T_L at the Bondville, Fort Peck, Table Mountain and Desert Rock stations, monthly average T_L values calculated from AOD and P_{wat} using Eq. (1) and (2) for all years in the study and the monthly average over all years of the calculated T_L. Atmospheric data was filtered for clear sky and low light before calculating T_L. The magnitude and shape of the historical and calculated T_L were similar for Bondville, Sioux Falls, Goodwin Creek and Penn State, but deviated for Fort Peck, Table Mountain and Dessert Rock. For all stations, T_L was greater in summer than winter.

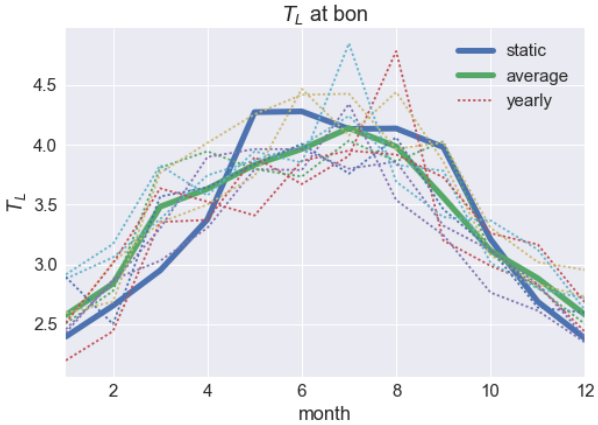

Fig. 1. Linke turbidity at Bondville, IL, from 2003 to 2012 calculated using filtered AOD and P_{wat} as dotted lines, the average for all years as solid green line and the 2003 historical values as solid blue line.

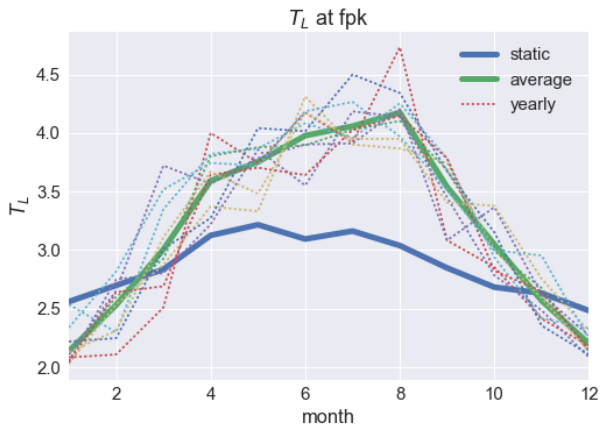

Fig. 2. Linke turbidity at Fort Peck, MT, from 2003 to 2012 calculated using filtered AOD and P_{wat} as dotted lines, the average for all years as solid green line and the 2003 historical values as solid blue line.

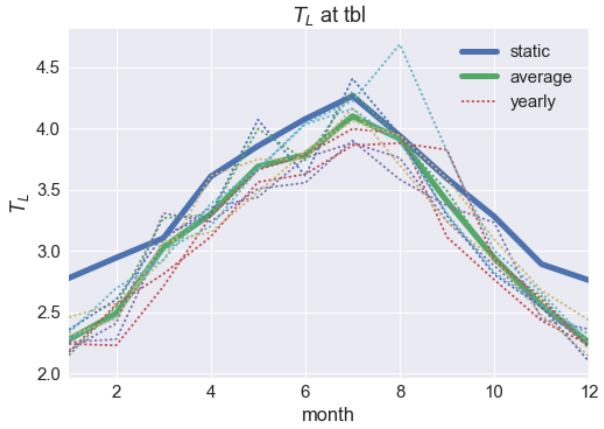

Fig. 3. Linke turbidity at Table Mountain, CO, from 2003 to 2012 calculated using filtered AOD and P_{wat} as dotted lines, the average for all years as solid green line and the 2003 historical values as solid blue line.

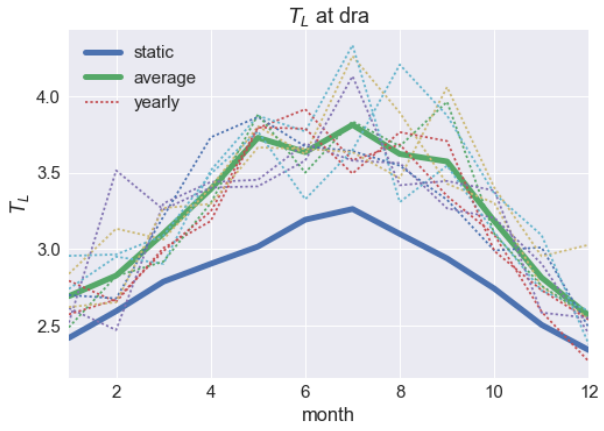

Fig. 4. Linke turbidity at Desert Rock, NV, from 2003 to 2012 calculated using filtered AOD and P_{wat} as dotted lines, the average for all years as solid green line and the 2003 historical values as solid blue line.

In Fig. 5 and 6, different clear sky models are compared to measured data at Bondville, IL on July 16th, 2006.

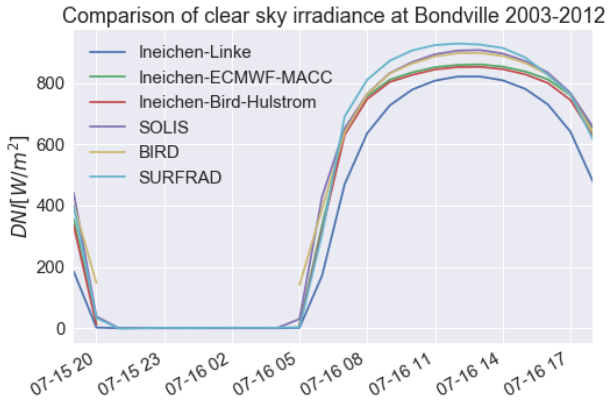

Fig. 5. Comparison of DNI at Bondville, IL on 7/16/2006 shows good agreement with Bird and Simplified Solis and poorer agreement with Ineichen-Perez using either historic or calculated T_L.

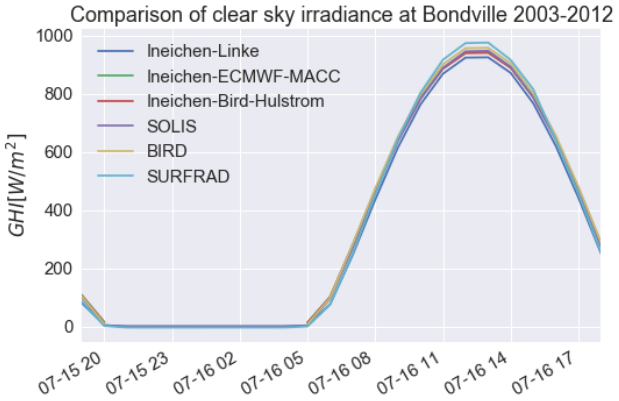

Fig. 6. Comparison of GHI at Bondville, IL on 7/16/2006. Bird and Simplified Solis with MACC data are slightly better than the historic or calculated T_L.

Fig. 7 to 14 show box plots of the distributions of average monthly relative errors, calculated using Eq. (5), for each clear sky model. The box bounds the the 2nd and 3rd quartiles, the whiskers show the 5% and 95% confidence bounds, the dashed red line is the mean, the solid black line is the median, and the flyers are values that fall outside of the confidence bounds. Fig. 7 and 8 show comparisons between clear sky models by year in different colors. Fig. 7 shows that there are no significant long term trends in DNI errors and no significant differences between models. The Ineichen-Perez model with static T_L shows no trend from year to year while the models using ECMWF MACC data show an increasing negative error with time. The Bird model had the largest mean yearly error. Fig. 8 shows that there are no significant long term trends in GHI errors and no significant differences between models. The Ineichen-Perez model with static T_L shows no trend from year to year while the models using ECMWF MACC data show an

increasing negative error with time. The Simplified Solis model had the largest mean yearly error.

From the year to year comparison, there does not appear to be significant difference between the use of static and real-time atmospheric data in clear sky predictions. The increasing yearly mean bias observed in DNI and GHI year to year box plots for models using real-time AOD and P_{wat} may be an artifact of the measured atmospheric data. For GHI the increase in relative mean bias error is less than 5%.

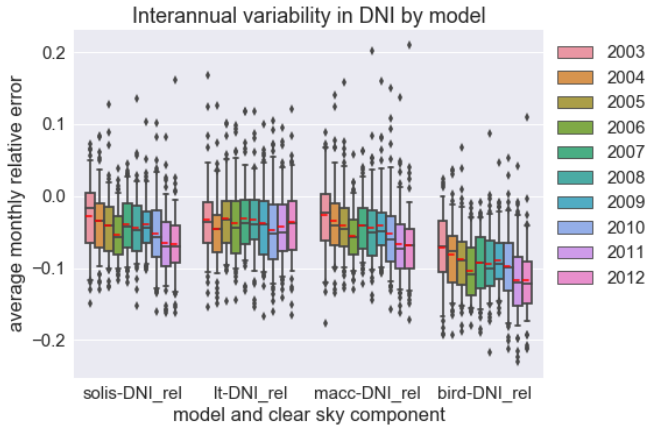

Fig. 7. Comparison of DNI errors at all stations by year (colors) and by model shows no statistical year to year variation and no statistical variation between models. The Ineichen-Perez model with static T_L has no trend from year to year while the models using ECMWF MACC show increasing mean error over time. The Bird model has the largest mean yearly error.

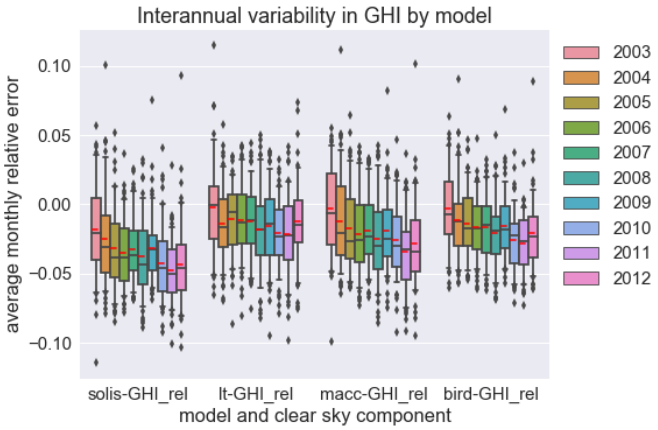

Fig. 8. Comparison of GHI errors at all stations by years (colors) and by model show no statistical year to year variation and no statistical variation between models. The Ineichen-Perez model with static T_L has no trend from year to year while the models using ECMWF MACC show increasing mean error over time. The Simplified Solis has the largest mean yearly error.

Fig. 9 and 10 show seasonal variations in error between clear sky models by month in different colors. The average monthly relative errors are grouped by month across all years. There are no significant differences in DNI errors by month or by model. The Bird model has the largest mean monthly errors. There is a seasonal bias in GHI errors for all models, including the Ineichen-Perez model with static T_L, so the seasonal bias cannot be an artifact of the AOD and P_{wat} measurements unless it arises from a common instrument error. The seasonal bias under-predicts GHI in summer, with a delta between the summer and winter mean error of less than 5%.

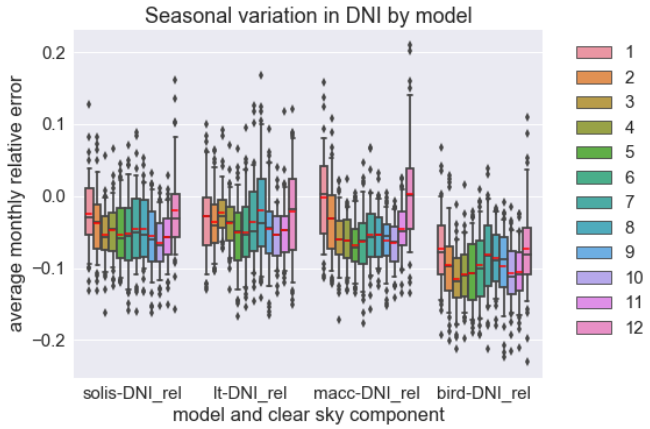

Fig. 9. Comparison of DNI errors at all stations by months (colors) shows no statistical differences by month or model.

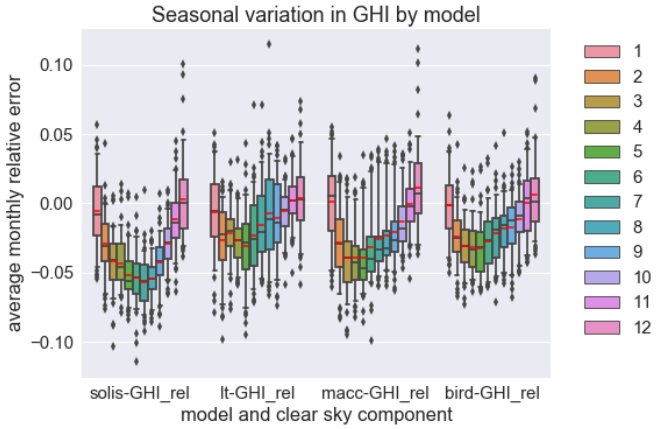

Fig. 10. Comparison of GHI errors at all stations by months (colors) show a seasonal bias, with a delta between summer and winter mean error of less than 5%.

Fig. 11 and 12 show regional variations in error between clear sky models by stations in different colors. The average monthly errors are grouped by station for all months and years. Fig. 8 shows the errors in DNI by station. The stations that had small differences between calculated T_L and static values have roughly consistent errors for all models. Two of the stations that had calculated T_L that deviated from the static values, Fort Peck and Desert Rock, show lower errors in both DNI and GHI with the Ineichen-Perez model using static T_L. The other station with calculated T_L that differed from the static values was the Table Mountain station, and it shows lower errors in both DNI and GHI with the Ineichen-Perez model using ECMWF MACC data. These three stations, Fort Peck, Desert

Rock and Table Mountain, were also the stations with the highest elevation and highest average DNI.

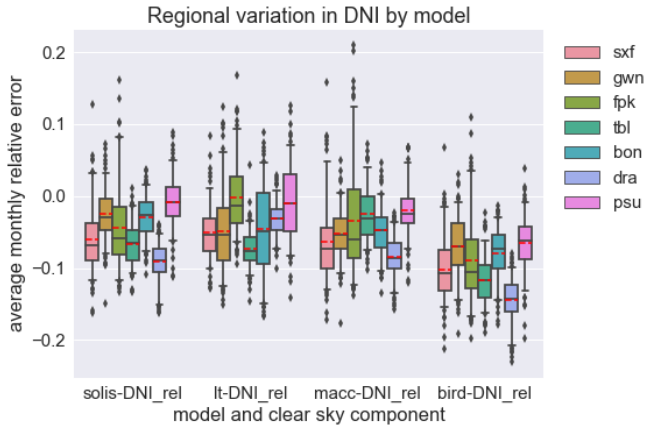

Fig. 11. Comparison of monthly DNI errors grouped by station (colors) show roughly the same mean error except for Fort Peck, Desert Rock, and Table Mountain, which were also the stations that had calculated T_L that differed from static values.

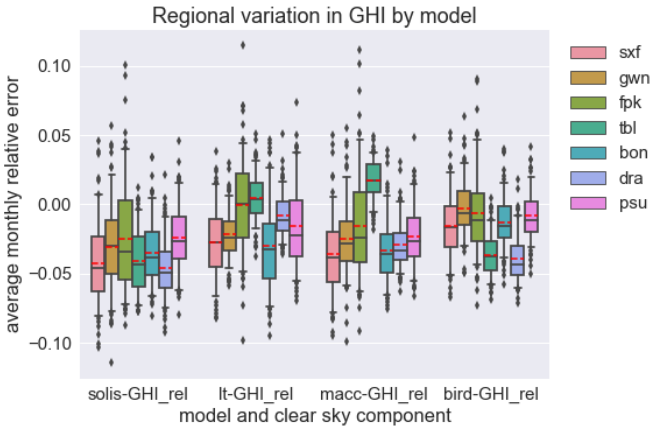

Fig. 12. Comparison of monthly GHI errors grouped by station (colors) show the mean error is less than 5% for all stations and models.

Fig. 13 and 14 show average relative error in DNI and GHI for all stations sorted by model. There were significant differences between GHI errors, although all models had average errors less than 5%. The Simplified Solis had the largest GHI error, and the Bird model had the lowest median error in this study but was not significantly different from the Ineichen-Perez model with either historical or real-time T_L. The Ineichen-Perez model with static T_L had the smallest errors in DNI, but was not statistically different from the Ineichen-Perez model with ECMWF MACC data or the Simplified Solis model. The Bird model had the largest DNI errors.

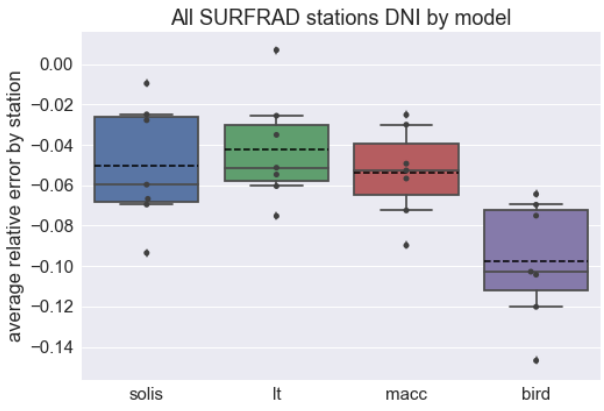

Fig. 13. Comparison of DNI errors for all stations by model show significant difference between Bird and other models.

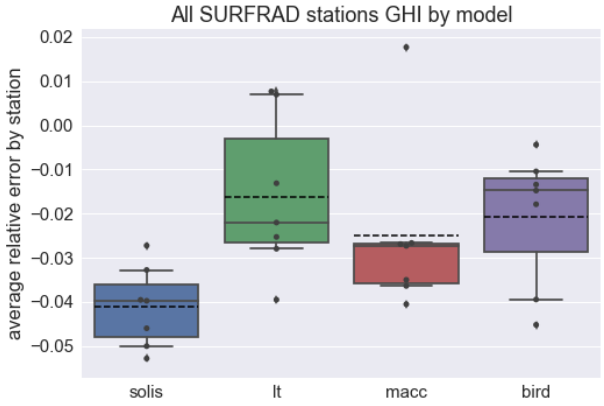

Fig. 14. Comparison of GHI errors for all stations by model show significant differences between the models in this study but all errors are less than 5%.

IV. Conclusions

A study of variations in clear sky irradiance due to AOD and P_{wat} has shown that for the seven stations and the ten-year period examined in this study there is no significant improvement in model accuracy when using real-time AOD and P_{wat} measurements. There is a seasonal bias in the GHI error that does not appear to be caused by the real-time AOD and P_{wat} measurements because it also appears in the errors from model using static T_L. The average monthly errors in GHI were not significantly different between models and were all less than 5%. The Ineichen-Perez model with static T_L had the lowest errors for DNI, but were not significantly different than the Simplified Solis model. The Bird model had significantly larger errors for DNI, but had the lowest GHI median error.

ACKNOWLEDGMENTS

Sandia National Laboratories is a multi-mission laboratory managed and operated by National Technology and Engineering Solutions of Sandia, LLC., a wholly owned subsidiary of Honeywell International, Inc., for the U.S. Department of Energy's National Nuclear Security Administration under contract DE-NA0003525.

REFERENCES

[1] P. Ineichen, "Validation of models that estimate the clear sky global and beam solar irradiance," *Sol. Energy*, vol. 132, pp. 332–344, 2016.

[2] P. Ineichen, "A broadband simplified version of the Solis clear sky model," *Sol. Energy*, vol. 82, no. 8, pp. 758–762, 2008.

[3] M. Sengupta and P. Gotseff, "Evaluation of Clear Sky Models for Satellite-Based Irradiance Estimates," 2013.

[4] R. E. Bird and R. L. Hulstrom, "Simplified Clear Sky Model for Direct and Diffuse Insolation on Horizontal Surfaces," 1981.

[5] R. E. Bird and R. L. Hulstrom, "Review, Evaluation, and Improvement of Direct Irradiance Models," *J. Sol. Energy Eng.*, vol. 103, no. 3, p. 182, 1981.

[6] D. R. Myers, "Solar radiation modeling and measurements for renewable energy applications: data and model quality," *Energy*, vol. 30, no. 9, pp. 1517–1531, Jul. 2005.

[7] R. L. Hulstrom, *Solar Resources*. MIT Press, 1989.

[8] W. F. Holmgren, R. W. Andrews, A. T. Lorenzo, and J. S. Stein, "PVLIB Python 2015," in *Photovoltaic Specialists Conference (PVSC), 2015 IEEE 42nd*, 2015, pp. 1–5.

[9] R. W. Andrews, J. S. Stein, C. Hansen, and D. Riley, "Introduction to the open source PV LIB for python Photovoltaic system modelling package," *2014 IEEE 40th Photovolt. Spec. Conf. PVSC 2014*, pp. 170–174, 2014.

[10] J. S. Stein, W. F. Holmgren, J. Forbess, and C. W. Hansen, "PVLIB: Open Source Photovoltaic Performance Modeling Functions for Matlab and Python," *IEEE 43rd Photovolt. Spec. Conf.*, pp. 3–8, 2016.

[11] R. Perez, P. Ineichen, K. Moore, M. Kmiecik, C. Chain, R. George, and F. Vignola, "A New Operational Satellite-to-Irradiance Model - Description and Validation," *Sol. Energy*, vol. 73, no. 5, pp. 307–317, 2002.

[12] P. Ineichen and R. Perez, "A new airmass independent formulation for the Linke turbidity coefficient," *Sol. Energy*, vol. 73, no. 3, pp. 151–157, Sep. 2002.

[13] F. Linke, "Transmissions-Koeffizient und Trubungsfaktor," *Beitrage zur Phys. der Atmosphare*, vol. 10, pp. 91–103, 1922.

[14] V. Cesnulyte, A. V. Lindfors, M. R. A. Pitkänen, K. E. J. Lehtinen, J. J. Morcrette, and A. Arola, "Comparing ECMWF AOD with AERONET observations at visible and UV wavelengths," *Atmos. Chem. Phys.*, vol. 14, no. 2, pp. 593–608, 2014.

[15] A. Angstrom, "On the Atmospheric Transmission of Sun Radiation and On Dust in the Air," *Geogr. Ann.*, vol. 11, pp. 156–166, 1929.

[16] A. ÅNGSTRÖM, "Techniques of Determinig the Turbidity of the Atmosphere," *Tellus A*, vol. 13, no. 2, pp. 214–223, 1961.

[17] F. Kasten, "A simple parameterization of the pyrheliometric formula for determining the Linke turbidity factor," *Meteorol. Rundschau*, vol. 33, pp. 124–127, 1980.

[18] F. Kasten, "The linke turbidity factor based on improved values of the integral Rayleigh optical thickness," *Sol. Energy*, vol. 56, no. 3, pp. 239–244, Mar. 1996.

[19] P. Ineichen, "Conversion function between the Linke turbidity and the atmospheric water vapor and aerosol content," *Sol. Energy*, vol. 82, no. 11, pp. 1095–1097, Nov. 2008.

[20] B. Molineaux, P. Ineichen, and N. O'Neill, "Equivalence of pyrheliometric and monochromatic aerosol optical depths at a single key wavelength.," *Appl. Opt.*, vol. 37, no. 30, pp. 7008–18, Oct. 1998.

[21] R. E. Bird and R. L. Hulstrom, "Direct Insolation Models," 1980.